Eddy self-similarity in turbulent pipe flow

L. H. O. Hellström,[1] T. Van Buren,[2] J. C. Vaccaro,[3] and A. J. Smits[1,*]
[1]*Mechanical and Aerospace Engineering, Princeton University, Princeton, New Jersey 08544, USA*
[2]*Mechanical Engineering, University of Delaware, Newark, Delaware 19716, USA*
[3]*Department of Engineering, Hofstra University, Hempstead, New York 11549, USA*

(Received 30 October 2023; accepted 15 March 2024; published 15 May 2024)

For wall-bounded turbulent flows, Townsend's attached eddy hypothesis proposes that the logarithmic layer is populated by a set of energetic and geometrically self-similar eddies. These eddies scale with a single length scale, their distance to the wall, while their velocity scale remains constant across all self-similar structures. To investigate the existence of such structures in fully developed turbulent pipe flow, stereoscopic particle image velocimetry measurements were performed in two parallel cross-sectional planes, spaced apart by a varying distance from 0 to $9.97R$, where R is the radius of the pipe, for friction Reynolds numbers $\mathrm{Re}_\tau = 1310$, 2430, and 3810. The instantaneous turbulence structures are sorted by width using an azimuthal Fourier decomposition and then azimuthally aligned to create a set of average eddy velocity profiles. The profiles exhibit geometric self-similar behavior in the azimuthal plane for eddies with spanwise length scales (λ_θ/R) spanning from 1.03 to 0.175. The streamwise similarity is then investigated using two-point correlations, where the structures exhibit a self-similar behavior with length scales (λ_θ/R) ranging from approximately 0.88 to 0.203. The candidate structures thereby establish full three-dimensional geometric self-similarity. In addition, the characteristic velocity magnitudes exhibit self-similarity within these ranges, using a velocity scale that is proportional to eddy size. This unexpected result is reconciled with the attached eddy hypothesis in terms of sampling probabilities.

DOI: 10.1103/PhysRevFluids.9.054607

I. INTRODUCTION

In the search for a physical model of wall-bounded turbulence, Ref. [1] introduced the "attached eddy" hypothesis where it was proposed that the constant stress region of a wall-bounded flow could be represented by a collection of geometrically self-similar eddies. The eddies were attached to the wall in the sense that their sizes were determined by their distance to the wall, y, and that they exhibited a range of sizes that grows with Reynolds number. The velocity field was then modeled as the linear superposition of the velocity fields induced by each of the attached eddies, where the magnitude of these individual fields was set by a single velocity scale (the friction velocity u_τ, where $u_\tau = \sqrt{\tau_w/\rho}$, τ_w is the wall shear stress and ρ is the fluid density). With these prescriptions, the model yields a constant stress region (corresponding in location to the logarithmic region in the mean velocity), and specific predictions for the normal stress distributions in the same region, in that the streamwise and spanwise Reynolds stress components are expected to follow a logarithmic behavior with respect to y, and the wall-normal component is constant.

*asmits@Princeton.EDU

Reference [2] extended this hypothesis to form what is now called the attached eddy model (AEM). Here the attached eddies of Townsend were complemented by a set of eddies that scale with the outer length scale (the boundary layer thickness δ, or the pipe flow radius R). They proposed that at high Reynolds numbers (where there is sufficient scale separation) there may exist an overlap region in wave-number space (k) between eddies that scale with y and eddies that scale with δ. The power spectral density function would then display a k^{-1} slope in this overlap region. Similarly, they proposed an overlap region in k between eddies that scale with y and eddies that scale with the Kolmogorov length scale η, which would give a region of $k^{-5/3}$ slope in the spectrum consistent with the inertial region of the energy cascade. When this model spectrum is integrated, the Reynolds stress components in the constant stress region follow the same scaling in y as that deduced by Townsend. In addition, the eddy velocity field in this region is expected to scale as u_τ. More details regarding the AEM are given by Ref. [3].

The support for these attached eddy models has focused primarily on verifying the predictions for the Reynolds stresses. For instance, experiments by Refs. [4,5] give strong backing for the predicted logarithmic variation of the streamwise component at high Reynolds number, while direct numerical computations (DNS) by Refs. [6,7] show that the predictions also hold for the spanwise and wall-normal components at considerably lower Reynolds numbers. Although the pipe and boundary layer experiments by Ref. [8] found no clear evidence for a k^{-1} slope in the spectrum, the streamwise Reynolds stress exhibited a clear logarithmic behavior with respect to y, as expected from the AEM. Reference [9] further showed that the probabilities of the eddy size populations are inversely proportional to their length scale, a key feature of the AEM.

However, it should be noted that the AEM is not universally accepted. In a recent work, Ref. [10] concluded that wall-normalized fluctuations are bounded as the Reynolds number approaches infinity giving support to the standard law of the wall. Furthermore, the evidence for the presence of self-similar structures themselves is still fairly limited. In the initial work, Ref. [1] assumed that the near-wall streaks found by Ref. [11] were self-similar, and modeled the statistical eddy as a double cone vortex. References [2,12] used the observations by Ref. [13] and modeled the self-similar eddies as hairpin vortices. Because the attached eddy model is linear, all nonlinear interactions between the self-similar motions need to be either small or included within each aggregate structure. In this respect, Ref. [14] showed that hairpin vortices of different sizes tend to align in the streamwise direction, creating the so-called hairpin packets or large-scale motions (LSMs). The LSMs can be thought to contain all nonlinear interactions, while the interaction between LSMs is linear. References [15,16] used these findings to generate an aggregated self-similar structure, where all nonlinear interactions are contained in the structure itself.

In this respect, proper orthogonal decomposition (POD), where each function is ordered based on its energy contribution, can be used to explore the eddy structure. For instance, Ref. [17] studied fully developed turbulent pipe flow at $\mathrm{Re}_\tau = u_\tau R/\nu = 2460$, where ν is the fluid kinematic viscosity. They acquired high-speed particle image velocimetry (PIV) data simultaneously in the streamwise (r, x) and cross-stream (r, θ) planes, revealing large structures with a spatiotemporal extent of 1-2R. These structures appeared to have characteristics very similar to the LSM, which was further supported by creating a conditionally averaged structure based on the occurrence/intensity of a given cross-stream snapshot POD mode. The resulting structures consisted of a combination of wall-attached and wall-detached large-scale components, which were shown to be associated with the most energetic modes. A pseudoalignment of these structures was observed, which together created structures with a spatiotemporal extent of about 6R, which is in accord with the findings of Ref. [18]. Furthermore, the method of using a Fourier decomposition in the azimuthal direction has been shown to be exceptionally well suited for finding large coherent structures in pipe flow. Building further on this, Ref. [19] performed a similar structure identification method on DNS data, and isolated the LSM velocity footprint as well as the associated pressure field. An important feature of the conditional mode is that, although the flow is no longer forced to be azimuthally periodic, the POD modes are only used to create the signal that conditions the averaging process. Consequently,

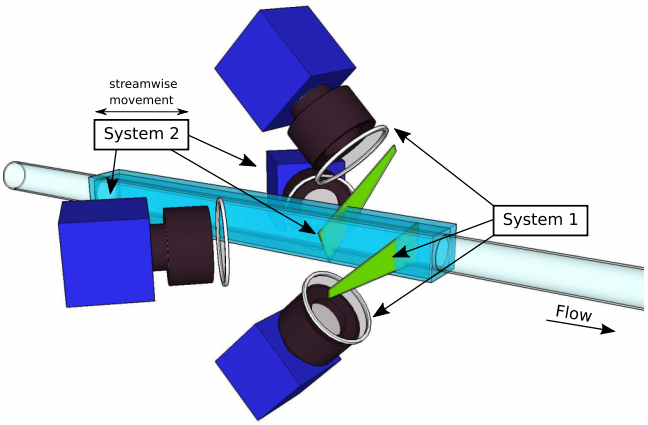

FIG. 1. The dual-plane stereo PIV experimental setup. The two systems are separated by orthogonally polarizing the two laser sheets and mounting polarizing filters to each camera. System 2 is mounted on a traverse such that ξ, the streamwise displacement between the two laser sheets, can be varied.

the structures are still aligned next to one another, showing that the azimuthal structure alignment is an inherent feature of the flow.

Reference [20] used similar experimental data as Ref. [17], but explored the scaling of the POD modes in terms of Townsend's attached eddy hypothesis. As a consequence of the available flow symmetries in pipe flow, they decomposed the azimuthal direction into Fourier modes, where the spanwise wavelength λ_θ defined the width of each structure. The radial direction was decomposed using POD and sorted by their energy contribution. For two Reynolds numbers, $\mathrm{Re}_\tau = 1330$ and 2460, they found that the first three POD modes (or eddies) exhibited self-similar behavior with respect to their azimuthal wavelengths, with their wall-normal length scales spanning a decade. This single length scale, derived from the azimuthal scaling, provided a complete description of the cross-sectional shape of the self-similar eddies. However, it is not yet clear to what degree the higher-order modes are self-similar, nor do we know which higher-order modes may be truncated altogether. In addition, although POD analysis is an excellent tool for identifying and analyzing geometrical self-similarity, it is not as useful for studying the scaling of the complete velocity field.

Therefore, we now extend this work to address the full three-dimensional similarity of the eddy motion shapes and their velocity scaling. The work uses a dual cross-plane PIV setup, where the distance between the two planes was varied in 21 steps, ranging from 0 to $9.97R$. The analysis is performed at three Reynolds numbers ($\mathrm{Re}_\tau \in \{1310,\ 2430,\ 3810\}$) and can be broken down into four parts: (i) deriving a representative structure; (ii) azimuthal/wall-normal similarity; (iii) velocity scaling; and (iv) azimuthal/streamwise similarity.

II. EXPERIMENTAL SETUP

The experiments were conducted in a $200D$ long pipe facility, consisting of seven, 1.2-m-long glass sections with an inner diameter $D = 38.1 \pm 0.025$ mm. The velocity field was simultaneously acquired in two cross-sectional planes using two stereoscopic PIV systems (2D-3C), with an adjustable streamwise displacement, ξ. Both PIV systems were triggered by an external signal such that data at each cross-sectional plane were acquired without temporal offset. As shown in Fig. 1, the first PIV system was held fixed and consisted of a pair of 5.5 Megapixel LaVision Imager sCMOS cameras arranged vertically above and below the pipe. The second system consisted of a pair of 4.0 Megapixel LaVision Imager SX cameras mounted horizontally along with a LaVision articulating

light delivery arm, and the system was mounted on a low friction rail and driven by a traverse such that it could be moved as a unit in the streamwise x-direction.

The working fluid was water seeded with 10 μm glass hollow spheres. The test section was enclosed by a rectangular acrylic box, filled with water to minimize the optical distortion due to refraction through the pipe wall, see Fig. 1. An access port was located immediately downstream of the test section to insert the stereo PIV calibration target while the pipe was filled with water. The target had 272 dots set in a rectangular grid, and was traversed 2 mm in each direction of the laser sheets, resulting in three calibration images for each camera.

A total of 21 data sets each containing 2000 image pairs were acquired for each Reynolds number. The streamwise distance between the two interrogation planes (ξ/R) was logarithmically varied, such that $(\xi/R) \in \{0.0; 0.0262; 0.0357; 0.0488; 0.0672; 0.0919; 0.126; 0.171; 0.234; 0.320; 0.438; 0.598; 0.818; 1.12; 1.53; 2.09; 2.86; 3.90; 5.34; 7.30; 9.97\}$. The separation distance was measured with a dial micrometer with a 12.7 μm resolution, and to reduce the overall error it was based on the cumulative displacement referenced from the origin. Following the procedure of Ref. [17], the two laser sheets were orthogonally polarized using two independent $l/2$-wave plates and each camera was subsequently equipped with linear polarizers such that they only identified particles situated within its system. Three Reynolds numbers were investigated, $\mathrm{Re}_\tau = u_\tau R/\nu \in \{1310; 2430; 3810\}$, or $\mathrm{Re}_D = U_b(2R)/\nu \in \{51,000; 102,100; 168,700\}$, where U_b is the bulk velocity. The systems were operated at $f = 10$ Hz, corresponding to a convective bulk displacement of $U_b/(Rf) \in \{7.05; 14.1; 23.3\}$ between snapshots, and all snapshots in the time series can therefore be considered statistically independent.

III. DATA ANALYSIS

We aim to identify a set of self-similar hierarchical structures that may be considered candidates for Townsend's attached eddy hypothesis. In the AEM it is assumed that the structures are placed along the wall and that there is a described distribution that orders smaller and larger structures. However, there is no restriction on the physical wall placement of these structures at a specific instance. Reference [16] used the approximation that the structures were randomly placed across the wall (later improved by assuming structures of the same size may not overlap). For our purposes, we need to reverse these steps, by reorganizing the seemingly randomly distributed structures contained within our data, such that they can be grouped, averaged, and analyzed.

Previous work showed that a spanwise Fourier decomposition of the fluctuating velocity field was a convenient initial step [20,21], and so we start there. This step acts as a sorting (or binning) procedure, where all structures with the same spanwise width are grouped and represented by their azimuthal Fourier mode number, m, indicative of the number of azimuthally aligned structures at each instance. To that end, consider Fig. 2(a) which shows a representative instantaneous velocity profile for, say, $m = 5$ at $\mathrm{Re}_\tau = 2430$, where y is measured from the wall ($y = R - r$). The azimuthal orientation of an instantaneous structure with respect to our $\theta = 0$ coordinate can be found from the phase of the complex velocity profile. At the particular instance shown in Fig. 2(a), we can see that both the real and imaginary components of the profile are negative, and of similar magnitude.

We will now derive a representative average eddy velocity profile for each mode m, represented by $u_\phi(m; r)$. References [20,22] performed a proper orthogonal decomposition in the radial direction and showed that the first few POD modes were self-similar. Here, we take an alternative approach and instead search for an average eddy velocity profile, u_ϕ, which, as a concept, lies closer to Townsend's hypothesis and also does not suffer from any truncation restrictions. As shown by Ref. [14], the large-scale motions come in a pseudoaligned manner, where areas of low-momentum fluid are followed by areas of high-momentum fluid, such that their long-time average goes to zero with respect to the mean. Hence, we cannot simply average the Fourier decomposed velocity field with respect to time, as it would average to zero, that is, $\langle \hat{u}(m; r, t) \rangle_t = 0$. This fundamental feature holds for the current data set; that is, there is no preferred azimuthal alignment for the eddies and their azimuthal distribution can, for all purposes here, be considered random. To create an average

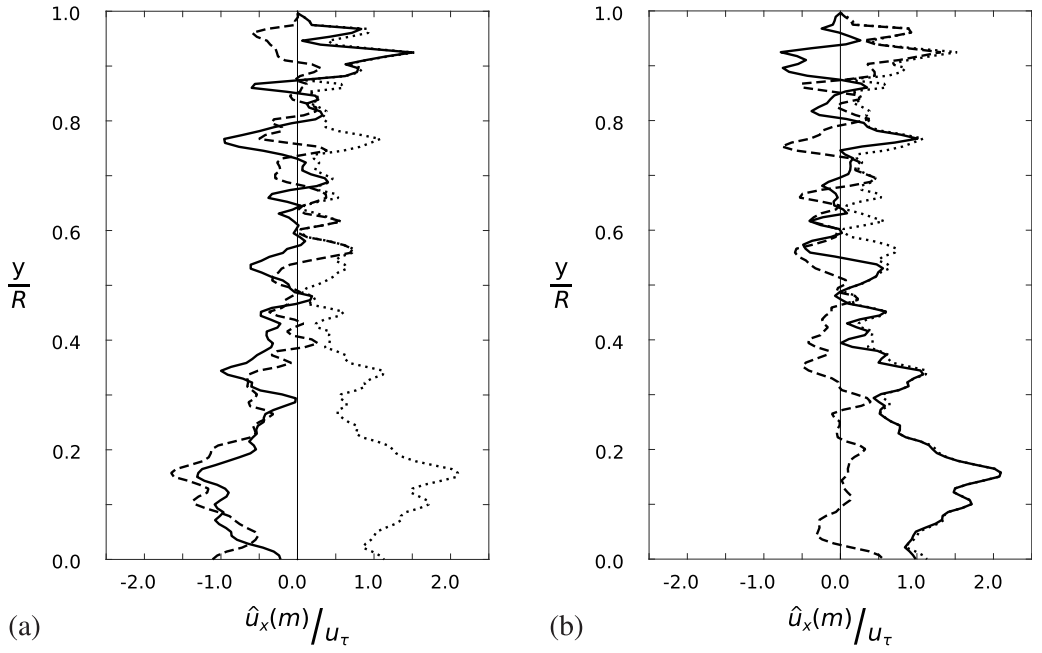

FIG. 2. A representative, instantaneous streamwise velocity ($\hat{u}_x$) profile for the fifth azimuthal mode ($m = 5$) and $\mathrm{Re}_\tau = 2430$. (a) original profile, (b) profile shifted in phase to optimize the real part. —, real part; −−, imaginary part; · · ·, absolute value (y is measured from the wall, $y = R - r$).

eddy velocity profile, u_ϕ, we will instead artificially align all structures of the same size before computing the average. We achieve this alignment by performing an azimuthal phase shift (ω) on each instantaneous velocity field, for each azimuthal mode number (m), such that its phase is 0. However, the phase for an azimuthally leaning structure changes with wall-normal distance and we need to consider a representative phase. From an algorithmic perspective, we therefore maximize the real part of the streamwise velocity profile in the l^2-norm sense by evaluating

$$\max_{\omega} \frac{\int_0^R (\Re(\hat{u}_x(m;r,t)e^{i\omega m}))^2 r dr}{\int_0^R (\Im(\hat{u}_x(m;r,t)e^{i\omega m}))^2 r dr}. \tag{1}$$

The phase shift procedure is illustrated in Fig. 2, where Fig. 2(a) is the original instantaneous velocity profile and Fig. 2(b) has been azimuthally shifted. The procedure considers and rotates each snapshot and azimuthal Fourier mode separately, and does not take account of any interaction between snapshots and scales. However, as each snapshot is taken to be statistically independent and Townsend's attached eddy hypothesis does not consider any scale interactions (or nonlinearities), these assumptions are in line with the generic approach taken in this work. One advantage of this procedure, compared to considering the absolute value of each instantaneous velocity field, is that the turbulence noise will average out instead of being accumulated.

The physical interpretation of the real or imaginary components of the Fourier decomposed velocity field is solely an artifact of the pipe coordinate system. If a (positive) structure has its peak value at $\theta = 0$, this would be represented as an imaginary component. If a (positive) structure starts at $\theta = 0$ this would be represented as a real component. However, because the pipe is axisymmetric, we may rotate the coordinate system without losing information on the structures.

This phase shift was applied to each instantaneous velocity field in the complete data set, for all azimuthal modes m. The representative eddy velocity profile $u_\phi(m;r)$ was obtained by performing a temporal average of the rectified velocity fields, and the results are shown in Fig. 3 as a function

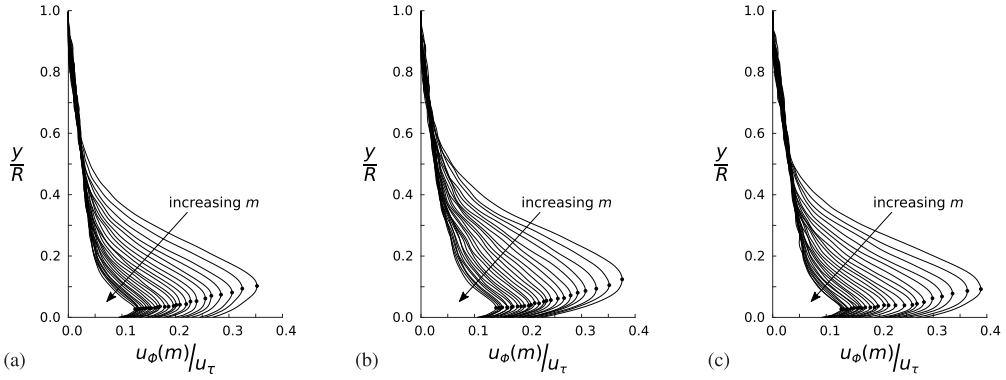

FIG. 3. The average eddy velocity profiles for all $m \in [10, 35]$. (a) $\mathrm{Re}_\tau = 1310$. (b) $\mathrm{Re}_\tau = 2430$. (c) $\mathrm{Re}_\tau = 3810$. The symbol • marks the peak location for each eddy velocity profile.

of the azimuthal mode number m. To assess the robustness of the phase alignment process the same procedure was performed while subjecting Eq. (1) to some modifications, namely, (i) introducing an adaptive integration limit $r \in (0, \lambda_\theta/2)$ and (ii) removing the radial weighting r in the l^2 integration. Neither of these changes imposed any noticeable changes to the peak location or the magnitude of the eddy velocity profiles.

We now need to verify that the averaging procedure that generated the eddy velocity profiles is meaningful. Because the structures are sorted by their spanwise width, it is crucial to inspect the repetition rate of the structures within each bin. Consider a hypothetical set of self-similar structures that collapses completely when scaled by their height and a common velocity scale (the friction velocity u_τ). If, however, their probability to occur decreases as their size increases, the no-activity space between consecutive structures of a given size would increase as their size decreases. This would lead to probability density functions (PDFs) of the streamwise velocity with more than one peak, representing the active and inactive zones, respectively. As an illustration, consider an $m = 5$ structure with a velocity strength of $10u_\tau$ that is present for a distance $1R$ and absent for a distance $1R$. Its average velocity strength would be $5u_\tau$. Now consider an $m = 10$ structure, with the same velocity strength $10u_\tau$ (that is, it has the same velocity scale). If this $m = 10$ structure is present for $0.5R$ and absent for $0.5R$, then its average would also be $5u_\tau$. However, we only know that the structure should be geometrically self-similar, and we cannot predict how often it occurs. If it were present for $0.5R$ and absent for $4.5R$, then the average strength would be u_τ, and it would incorrectly appear as a weaker structure. Thus, the averaging process used to estimate their strength (that is, their velocity scale) must also account for their probability of occurrence.

Figure 4 shows the velocity PDFs for three different structure sizes, $m \in \{10, 15, 20\}$, for all three Reynolds numbers. For consistency, each PDF is evaluated at the eddy peak location y_{MAX} as found from the data shown in Fig. 3. We consider the Fourier-transformed velocity field, which is complex, and the PDF is visualized in the complex plane. The corresponding eddy peak velocity found in Fig. 3 is shown with a solid white circle in Fig. 4, and it consistently falls in the vicinity of the PDF peak. There is only one peak, and so all eddies of the same width will from here on be represented by their average velocity profiles, as shown in Fig. 3.

IV. EDDY SELF-SIMILARITY

We begin by considering the azimuthal direction. As previously indicated, the azimuthal direction is already a self-similar dimension, that is, all structures are (based on the Fourier decomposition) forced sine waves. When decomposing a flow using POD, the basis functions are optimal in that the average turbulent kinetic energy of the first n modes is maximized. If a direction is statistically

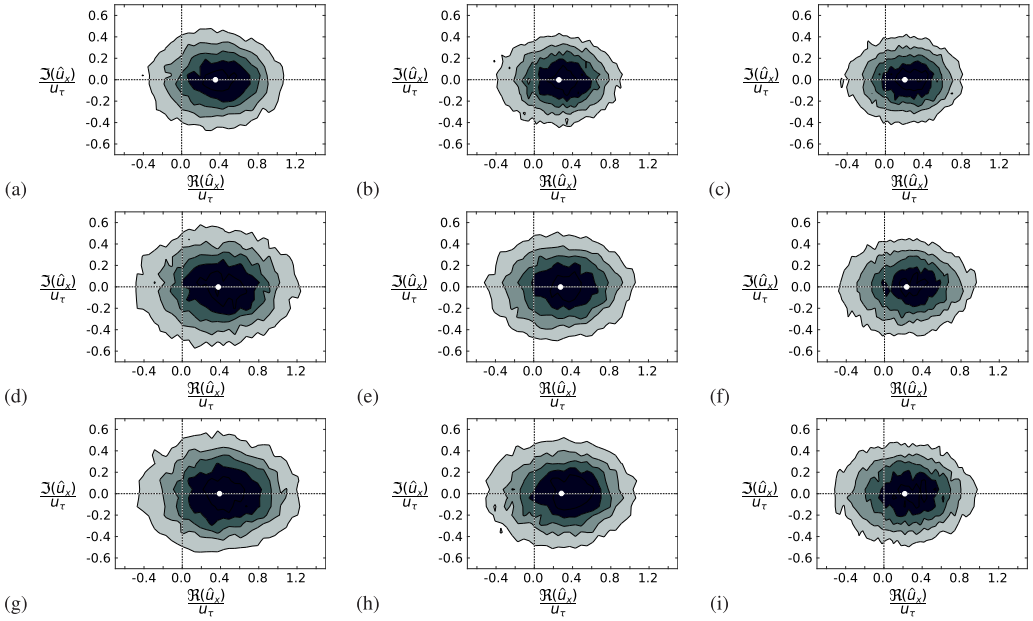

FIG. 4. PDFs of the streamwise velocity component u_x, evaluated at the peak eddy velocity location found in Fig. 3 (real and imaginary parts). The corresponding peak eddy velocity found in Fig. 3 is shown with a solid white circle. (a) $\mathrm{Re}_\tau = 1310$, $m = 10$. (b) $\mathrm{Re}_\tau = 1310$, $m = 15$. (c) $\mathrm{Re}_\tau = 1310$, $m = 20$. (d) $\mathrm{Re}_\tau = 2430$, $m = 10$. (e) $\mathrm{Re}_\tau = 2430$, $m = 15$. (f) $\mathrm{Re}_\tau = 2430$, $m = 20$. (g) $\mathrm{Re}_\tau = 3810$, $m = 10$. (h) $\mathrm{Re}_\tau = 3810$, $m = 15$. (i) $\mathrm{Re}_\tau = 3810$, $m = 20$. Each PDF is scaled by its peak value and is shown with contour levels $\{0.2, 0.4, 0.6, 0.8\}$.

homogeneous and periodic (or infinite), then the POD modes are reduced to a Fourier series (or Fourier transform). As a consequence of the axisymmetry of the pipe, the azimuthal Fourier modes are therefore the optimal decomposition, in a POD sense, in this direction. We will build on this observation and assume that the eddy width can be represented by the azimuthal wavelength and that this wavelength can be used as the characteristic length scale. The eddy width can then be defined as $\lambda_\theta = 2\pi(R - y_{\mathrm{MAX}})/m$, where y_{MAX} is the wall-normal location where the eddy velocity profile has its maximum, as seen in Fig. 3.

As to the wall-normal direction, Figs. 5(a) and 5(b) show the averaged eddy profiles scaled in outer and eddy-size coordinates, respectively. Similarly to Fig. 3, $u_\phi(m; r)$ represents the streamwise component of the eddy structures, for each mode m. The eddy profiles are shown for the range $m \in [5,\ 35]$, which corresponds to $\lambda_\theta/R \in [1.03,\ 0.175]$ for $\mathrm{Re}_\tau = 1310$; $\lambda_\theta/R \in [1.02,\ 0.174]$ for $\mathrm{Re}_\tau = 2430$; and $\lambda_\theta/R \in [1.05,\ 0.175]$ for $\mathrm{Re}_\tau = 3810$.

To define a cutoff between inner and outer regions, consider simple spherical eddies, where each positive eddy is flanked by two negative eddies (and vice versa). The azimuthal wavelength will span the width of a positive and a negative structure combined, and their characteristic height will consequently be $0.5\lambda_\theta$. We use this example to define the outer region of the eddies as 3 times the height of the eddy or $1.5\lambda_\theta$ so that the near-wall behavior would not influence the outer flow behavior. In Fig. 5(a) the outer section of each eddy is highlighted with a solid line while the inner region is dotted, and we can see a complete similarity collapse for all profiles and Reynolds numbers in this region ($y/R > 1.5\lambda_\theta/\mathrm{R}$).

The inner region should, according to Townsend, be geometrically scaled by the eddy size, and in Fig. 5(b) we see a reasonable collapse in the wall-normal location of the peaks of all the eddy velocity profiles for all Reynolds numbers (located approximately at $y/\lambda_\theta = 0.2$). In addition, for

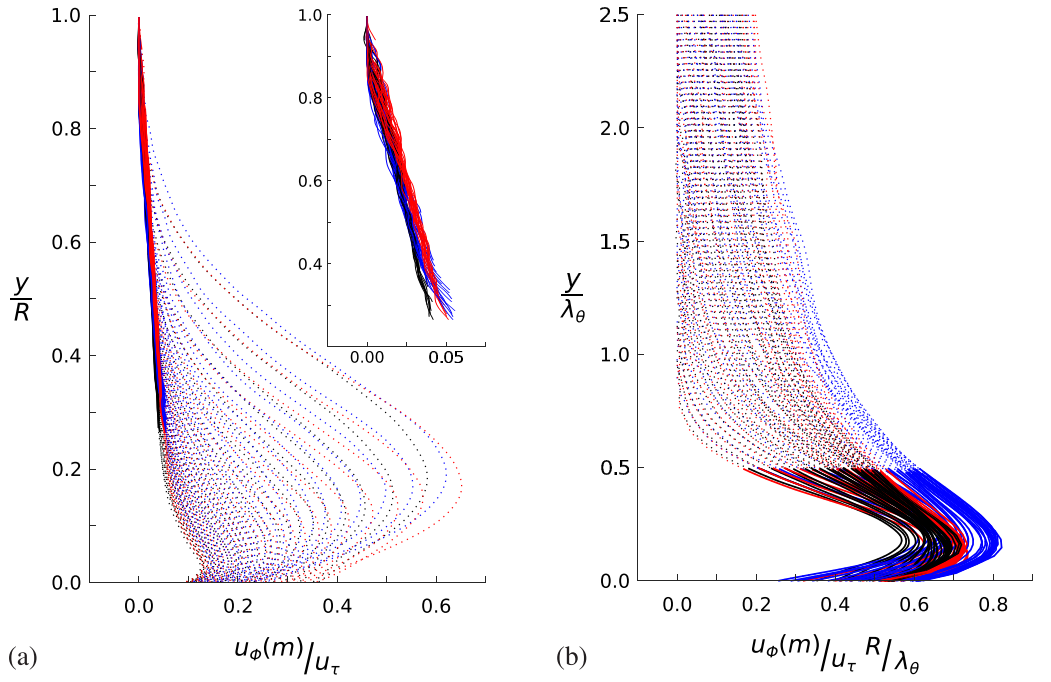

FIG. 5. Eddy velocity profiles for all $m \in [5, 35]$. Profiles for $\mathrm{Re}_\tau = \{1310, 2430, 3810\}$ are shown in black, blue, and red line plots, respectively. (a) Profiles scaled with outer coordinates, where the outer section of each profile ($y \geqslant 1.5\lambda_\theta$) is highlighted with a solid line. The insert shows a zoomed view of the outer section of the structures and highlights the close collapse in this region. (b) Profiles scaled with eddy-size coordinates, where the inner section of each profile ($y \leqslant 0.5\lambda_\theta$) is highlighted with a solid line.

comparison with the AEM, we need to consider the number of eddies per unit area, which means that the correct velocity scale should be $u_\phi \propto y u_\tau/R \propto \lambda_\theta u_\tau/R$. Figure 5(b) provides some support for this linear scaling, where the peak in the scaled velocity has a standard deviation of less than 10% around a mean value of approximately 0.68. There is no Reynolds number trend, and within each data set there is no clear link to structure size. The deviations from a more precise collapse may reflect the influence of the eddy convection velocity, which is close to the local mean velocity. Alternatively, the deviations might originate from the nondiscriminatory averaging approach, which may include structures not driven by inertial forces and consequently could help dictate the eddy velocity profile.

Thus, we appear to have achieved a plausible self-similar eddy scaling for the azimuthal and wall-normal directions and recognized a possible self-similar behavior for the eddy velocity profiles. The fourth, and last, dimension is the streamwise length of each eddy, which will now be examined using two-point correlations between the two PIV interrogation planes. The correlation map considers the Fourier-transformed velocity fields, with one fixed reference point located at y_{MAX}. That is, we define

$$\rho(\eta, m, \xi) = \frac{\frac{1}{T}\sum_{t=1}^{T} \hat{u}_x(y_{\mathrm{MAX}}, m, x_0, t)\hat{u}_x^*(y_{\mathrm{MAX}} + \eta, m, x_0 + \xi, t)}{\| \hat{u}_x(y_{\mathrm{MAX}}, m, x_0, t) \|_t}, \tag{2}$$

where $\wedge$, $*$, and $\| \cdot \|_t$ represent the Fourier transformed velocity field, its complex conjugate, and the l^2-norm with respect to time, respectively, and η and ξ are the wall-normal and streamwise spatial shifts in the two-point correlations. The two velocity fields used in these correlation maps have not been subject to any azimuthal phase shift since it is unnecessary; the two planes capture

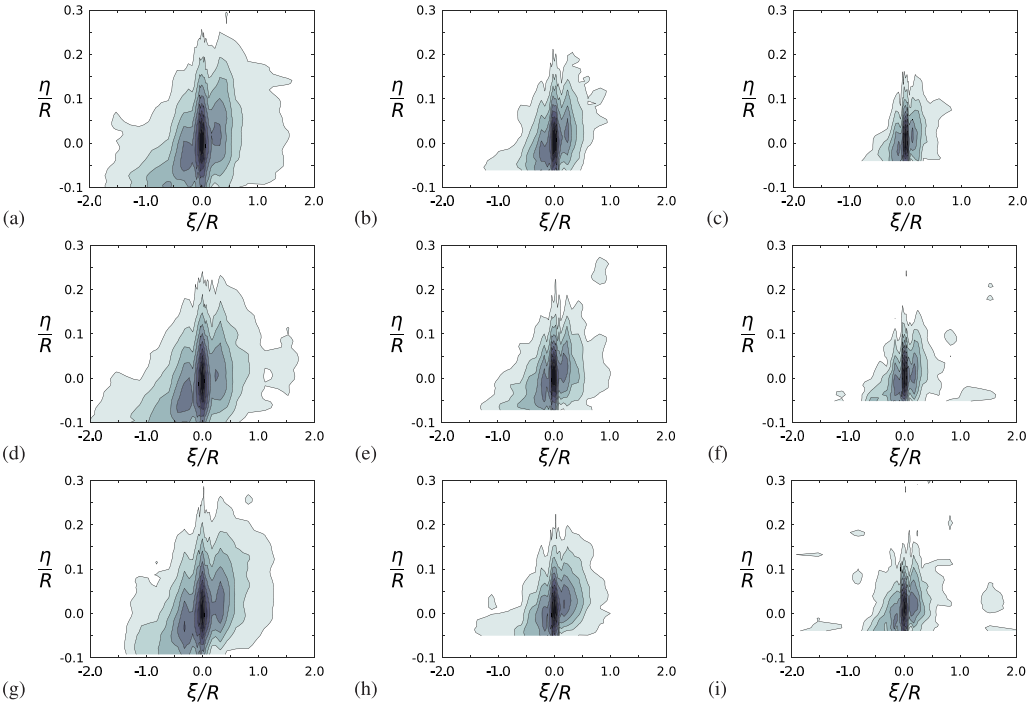

FIG. 6. Absolute value of the correlation maps described in Eq. (2). The wall-normal reference point y_{MAX} is located at the origin, with the wall approaching the origin for decreasing structure sizes. (a) $\mathrm{Re}_\tau = 1310$, $m = 10$. (b) $\mathrm{Re}_\tau = 1310$, $m = 15$. (c) $\mathrm{Re}_\tau = 1310$, $m = 20$. (d) $\mathrm{Re}_\tau = 2430$, $m = 10$. (e) $\mathrm{Re}_\tau = 2430$, $m = 15$. (f) $\mathrm{Re}_\tau = 2430$, $m = 20$. (g) $\mathrm{Re}_\tau = 3810$, $m = 10$. (h) $\mathrm{Re}_\tau = 3810$, $m = 15$. (i) $\mathrm{Re}_\tau = 3810$, $m = 20$. Each correlation map is scaled by its peak value and is shown with contour lines ranging from 0.1 to 0.9 with 0.1 increments.

the same structure in their respective views, and so would be subject to either the same phase shift or none at all.

The absolute values of the correlation for $m \in \{10,\ 15,\ 20\}$ are mapped in Fig. 6. All correlations were constructed using points from the two independent planes, including the auto-correlations ($\xi = 0$), allowing any sampling noise to average out. The reference planes were inter-changed to construct both the upstream and downstream sections of the correlation maps. These absolute value correlation maps reveal a streamwise leaning structure, similar to the large-scale motions, with a decrease in height and length as their width decreases.

When the absolute correlation maps are scaled using the eddy length scale λ_θ, as in Fig. 7, the structures exhibit a convincingly self-similar behavior, where the structure height and length are approximately equal. We can also see a weak repetition within each structure, represented by a secondary (weaker) correlation peak located at $\xi/\lambda_\theta = \pm 0.5$. The observed secondary peaks are consistent with the proposal that the large-scale motions (LSMs) are constructed from a set of streamwise aligned hairpin vortices [14]. It can also be seen that, in accordance with Ref. [14], the upstream correlation peak at $\xi/\lambda_\theta = -0.5$ is attached to the wall, while the downstream correlation peak at $\xi/\lambda_\theta = +0.5$ has detached and could be considered a more mature sub-structure. Reference [14] further found that the typical slope of the envelope of the LSM was 11°, subject to some variation due to the size and maturity of the LSM, with larger and more mature structures exhibiting a steeper slope. Figure 7 shows that the inclination for each identified structure is close to 11°, again supporting the theory that the identified structures are the LSMs.

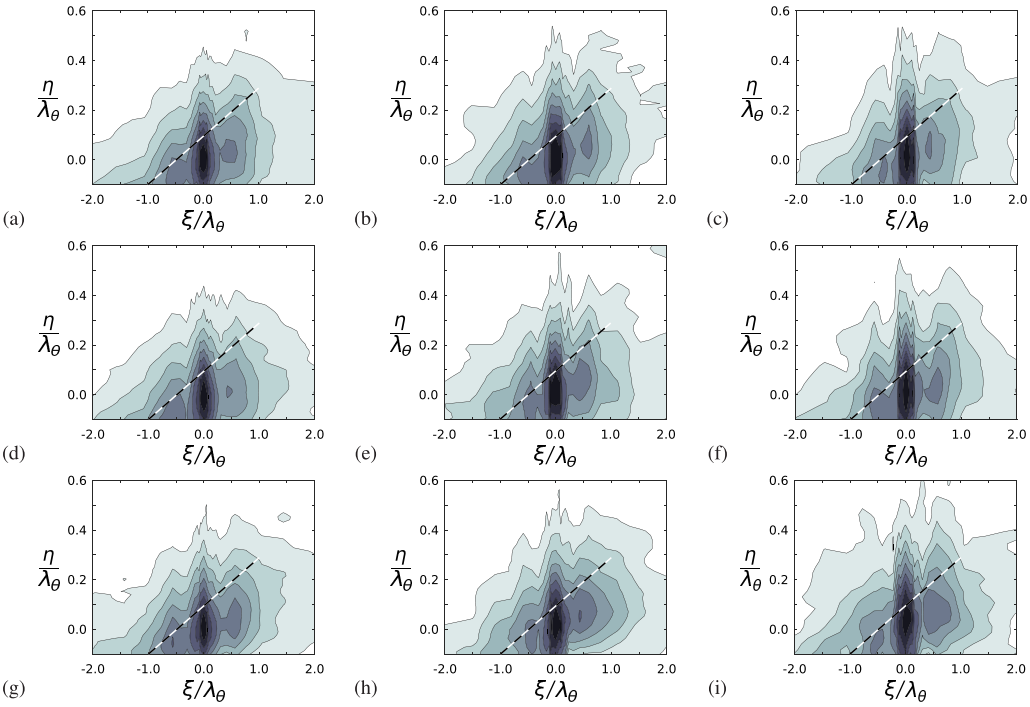

FIG. 7. Absolute value of the scaled correlation maps. The wall-normal reference point y_{MAX} is located at the origin, with the wall approaching the origin for decreasing structure sizes. (a) $\mathrm{Re}_\tau = 1310$, $m = 10$. (b) $\mathrm{Re}_\tau = 1310$, $m = 15$. (c) $\mathrm{Re}_\tau = 1310$, $m = 20$. (d) $\mathrm{Re}_\tau = 2430$, $m = 10$. (e) $\mathrm{Re}_\tau = 2430$, $m = 15$. (f) $\mathrm{Re}_\tau = 2430$, $m = 20$. (g) $\mathrm{Re}_\tau = 3810$, $m = 10$. (h) $\mathrm{Re}_\tau = 3810$, $m = 15$. (i) $\mathrm{Re}_\tau = 3810$, $m = 20$. Each correlation map is scaled by its peak value and is shown with contour lines ranging from 0.1 to 0.9 with 0.1 increments. Dashed line represents an 11° slope, as seen for LSMs [14].

In addition to visual comparisons based on Fig. 7, we can pursue a more objective measure of the self-similarity in the streamwise direction by comparing the streamwise correlation of each eddy, evaluated at the eddy-specific wall distance y_{MAX}. Figure 8 shows the correlations for all azimuthal modes in the range $m \in [5, 35]$. Symmetry was not enforced in any way, and so the inherent symmetry of the correlation profiles can be seen as indicating a well-converged data set. There is a clear similarity between the correlation profiles, independent of Reynolds number, although some spread is seen in the tails.

To examine the correlation tails in more detail, we first define the streamwise eddy length as the distance between the upstream and downstream ends of the correlation where the correlation is above a chosen threshold. Figure 9 shows the streamwise length of each eddy, normalized by its width, for three different thresholds, $\rho = 0.08$, 0.10, and 0.12. The scaled eddy length remains reasonably constant for $m \in [6, 30]$, and it is insensitive to eddy size, and the chosen threshold. This range of m corresponds to eddy sizes (λ_θ/R) between [0.885, 0.203], [0.870, 0.203], and [0.890, 0.203] for Reynolds numbers 1310, 2430, and 3810, respectively. Due to the nature of the Fourier transforms, these lengths correspond to a positive structure and its negative neighbor, and each structure width should be taken as $\lambda_\theta/2$, if we take the width of a LSM to be the distance between its widest legs. However, the departure from this scaling for the smaller eddies is most likely due to the limited streamwise resolution along with the volumetric velocity averaging in the PIV process. For instance, the smallest eddy width of $0.2R$ in the current setup corresponds to 3.8 mm, compared to the 1 mm thick laser sheet. It is therefore possible that the self-similar behavior might extend to even smaller structures if investigated using different data acquisition tools.

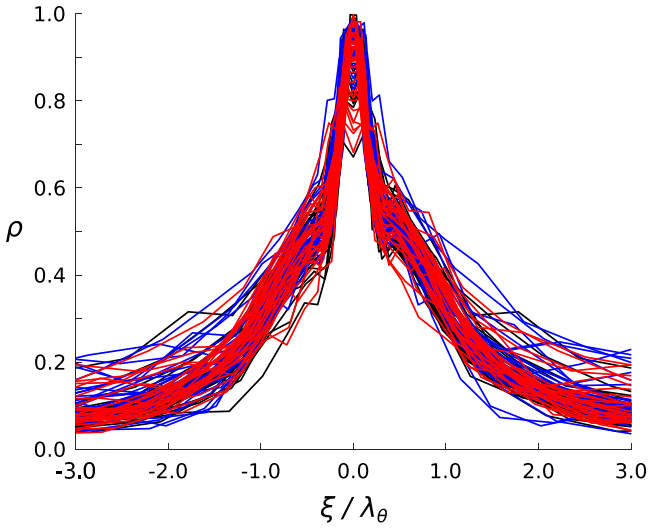

FIG. 8. Absolute value of the correlation maps, evaluated at the eddy-specific wall-distance y_{MAX}, where the eddy velocity profile has its maximum. Showing all profiles for the range $m \in [5,\ 35]$. $\mathrm{Re}_\tau = \{1310,\ 2430,\ 3810\}$ are shown in black, blue, and red, respectively.

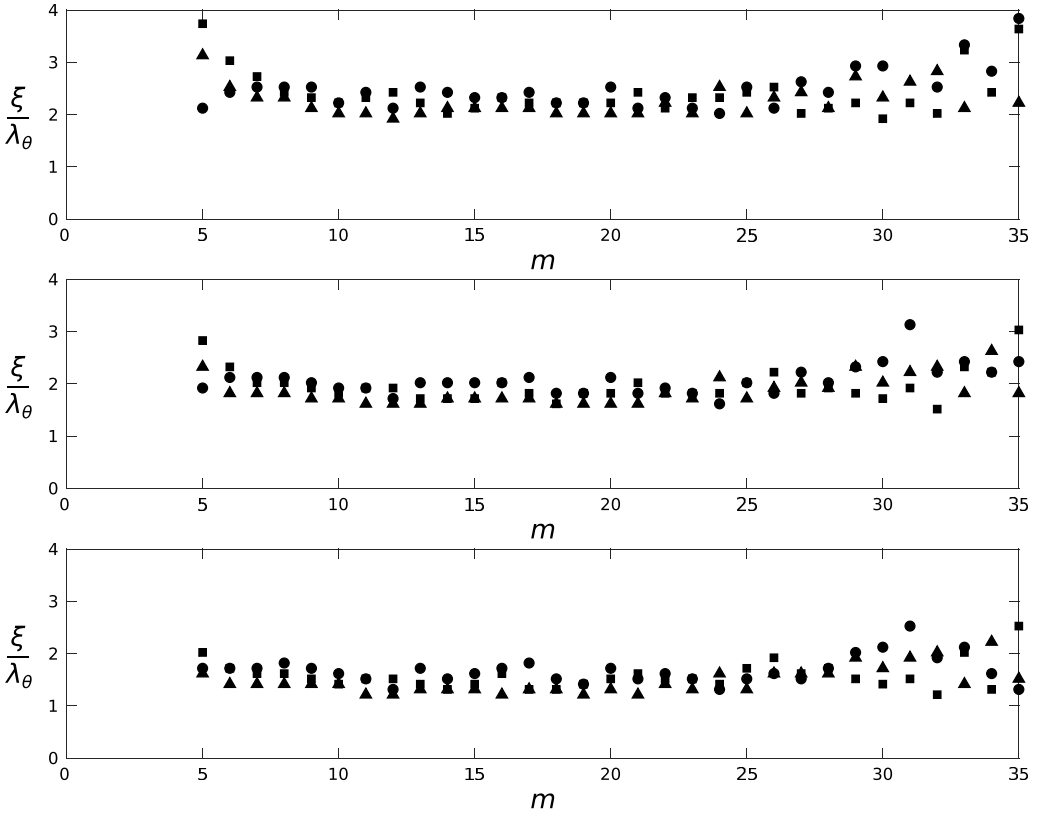

FIG. 9. Streamwise correlation lengths, evaluated from the profiles in Fig. 8. The considered thresholds are: (a) $\rho = 0.08$, (b) 0.10, (c) 0.12. ▲ $\mathrm{Re}_\tau = 1310$; ■ $\mathrm{Re}_\tau = 2430$; ● $\mathrm{Re}_\tau = 3810$.

Finally, to compare our findings with existing literature, Fig. 9 indicates that $\xi/\lambda_\theta \approx 1.5$–$2$ for the three correlation levels and three Reynolds numbers shown. From Fig. 5(b) we find that $y/\lambda_\theta \approx 0.2$, and deduce that $\xi/y \approx 7.5$–10, which is in reasonable agreement with the aspect ratio of 7 measured by Ref. [23] in pipes and boundary layers at much higher Reynolds numbers. The same ratio of 7 can also be inferred from the results obtained from DNS of pipe flow at $\mathrm{Re}_\tau = 685$ [19], suggesting that it is independent of Reynolds number and common to pipes and boundary layers.

V. DISCUSSION AND CONCLUSIONS

The eddy scaling of fully developed turbulent pipe flow was investigated in the context of the attached eddy model. The eddy structure was identified using Fourier decomposition in the spanwise plane, and two-point correlations in the streamwise plane. In the spanwise plane, the average eddy velocity profile corresponding to a given azimuthal mode was created by azimuthally aligning the structures. The eddy velocity profiles displayed an inner and outer region, where the outer region obeyed the classical outer layer scaling using pipe radius and friction velocity. For the inner region, the height of the eddy velocity profiles, for $m \in [5,\ 35]$, were scaled by their characteristic width (azimuthal wavelength), as expected for attached eddies. Within this range, the structure sizes ranged approximately $\lambda_\theta/R \in [1.03,\ 0.175]$, where the length-scale ratio was 5.89. The characteristic eddy velocity magnitude could also be predicted because the data spans the spanwise/wall-normal plane, rather than only the wall-normal dimension as typically sampled. In the streamwise direction, the two-point correlation showed that the streamwise length of these eddies scaled using their characteristic width so that the structures display a fully self-similar behavior (for $m \in [6,\ 30]$. The self-similar range can also be expressed as $\lambda_\theta/R \in [0.885,\ 0.203]$, $[0.870,\ 0.203]$, and $[0.890,\ 0.203]$, for Reynolds numbers 1310, 2430, and 3810, respectively. For this structure range, the resolved length-scale ratio is 4.3, while the volumetric ratio is 1 : 80. The correlations also revealed the presence of smaller repetitive structures within the larger comportment, in accordance with the expected behavior of the large-scale motions. The detected structures showed no significant Reynolds number effects over the range of Reynolds numbers studied here.

Finally, we note that the attached eddy model proposes a simplified framework for how turbulence can be viewed. It is a linear model and all nonlinearities must either be neglected or included in the base structure. A potent base-structure therefore includes the nonlinearities, and consequently must also be allowed to be composed of a range of smaller structures, as suggested by the findings presented here.

ACKNOWLEDGMENT

This work was supported under ONR Grants No. N00014-15-1-2402 and No. N00014-17-1-2309.

[1] A. A. Townsend, *The Structure of Turbulent Shear Flow* (Cambridge University Press, Cambridge, UK, 1976).

[2] A. E. Perry, S. Henbest, and M. S. Chong, A theoretical and experimental study of wall turbulence, J. Fluid Mech. **165**, 163 (1986).

[3] I. Marusic and J. P. Monty, Attached eddy model of wall turbulence, Annu. Rev. Fluid Mech. **51**, 49 (2019).

[4] M. Hultmark, M. Vallikivi, S. C. C. Bailey, and A. J. Smits, Turbulent pipe flow at extreme Reynolds numbers, Phys. Rev. Lett. **108**, 094501 (2012).

[5] I. Marusic, J. P. Monty, M. Hultmark, and A. J. Smits, On the logarithmic region in wall turbulence, J. Fluid Mech. **716**, R3 (2013).

[6] J. Jimenez and S. Hoyas, Turbulent fluctuations above the buffer layer of wall-bounded flows, J. Fluid Mech. **611**, 215 (2008).
[7] M. Lee and R. D. Moser, Direct numerical simulation of turbulent channel flow up to $\mathrm{Re}_\tau = 5200$, J. Fluid Mech. **774**, 395 (2015).
[8] M. Vallikivi, B. Ganapathisubramani, and A. J. Smits, Spectral scaling in boundary layers and pipes at very high Reynolds numbers, J. Fluid Mech. **771**, 303 (2015).
[9] J. Hwang and H. J. Sung, Wall-attached structures of velocity fluctuations in a turbulent boundary layer, J. Fluid Mech. **856**, 958 (2018).
[10] X. Chen and K. R. Sreenivasan, Reynolds number asymptotics of wall-turbulence fluctuations, J. Fluid Mech. **976**, A21 (2023).
[11] S. J. Kline, W. C. Reynolds, F. A. Schraub, and P. W. Runstadler, The structure of turbulent boundary layers, J. Fluid Mech. **30**, 741 (1967).
[12] A. E. Perry and M. S. Chong, On the mechanism of wall turbulence, J. Fluid Mech. **119**, 173 (1982).
[13] M. R. Head and P. Bandyopadhyay, New aspects of turbulent boundary-layer structure, J. Fluid Mech. **107**, 297 (1981).
[14] R. J. Adrian, C. D. Meinhart, and C. D. Tomkins, Vortex organization in the outer region of the turbulent boundary layer, J. Fluid Mech. **422**, 1 (2000).
[15] I. Marusic, On the role of large-scale structures in wall turbulence, Phys. Fluids **13**, 735 (2001).
[16] J. D. Woodcock and I. Marusic, The statistical behaviour of attached eddies, Phys. Fluids **27**, 015104 (2015).
[17] L. H. O. Hellström, B. Ganapathisubramani, and A. J. Smits, The evolution of large-scale motions in turbulent pipe flow, J. Fluid Mech. **779**, 701 (2015).
[18] K. C. Kim and R. J. Adrian, Very large-scale motion in the outer layer, Phys. Fluids **11**, 417 (1999).
[19] L. H. O. Hellström and A. J. Smits, Structure identification in pipe flow using proper orthogonal decomposition, Phil. Trans. R. Soc. Lond. A **375**, 20160086 (2017).
[20] L. H. O. Hellström, I. Marusic, and A. J. Smits, Self-similarity of the large-scale motions in turbulent pipe flow, J. Fluid Mech. **792**, R1 (2016)
[21] Y. Hwang, Statistical structure of self-sustaining attached eddies in turbulent channel flow, J. Fluid Mech. **767**, 254 (2015).
[22] L. H. O. Hellström, T. Van Buren, J. C. Vaccaro, and A. J. Smits, On the existence of self-similar structures in turbulent pipe flow, in *Proceedings of the International Symposium on Turbulence and Shear Flow Phenomena* (Chicago, IL, 2017).
[23] R. Baidya, W. J. Baars, S. Zimmerman, M. Samie, R. J. Hearst, E. Dogan, L. Mascotelli, X. Zheng, G. Bellani, A. Talamelli *et al.*, Simultaneous skin friction and velocity measurements in high Reynolds number pipe and boundary layer flows, J. Fluid Mech. **871**, 377 (2019).